JOINT INSTITUTE FOR NUCLEAR RESEARCH
Flerov Laboratory of Nuclear Reactions

FINAL REPORT ON THE INTEREST PROGRAMME

Production and Spectroscopic Investigation of New Neutron-Rich Isotopes Near the Neutron N=126 Shell Closure Using the Multinucleon Transfer Reactions

Supervisor:
Mr. Viacheslav Vedeneev

Student:
Kadir Özgür Hanci, Turkiye
Middle East Technical University

Participation period:
March 03 – April 20, Wave 12

Dubna, 2025

Contents

Abstract

This report presents alpha-decay data from three nuclear reactions: Ar-40+Sm-148, Ar-40+Er-166, and Ca-48+Pu-242, measured using the MASHA mass-separator system. The setup combines thermal release, ECR ionization, and magneto-optical separation to detect short-lived, neutron-rich isotopes. Energy spectra and position–energy heatmaps were obtained using a silicon-strip detector, enabling identification of isotopes including Hg-180 to Hg-185 and Rn-201 to Rn-205. Measured alpha energies showed strong agreement with theoretical values, and decay events appeared as distinct peaks and spatial clusters on the detector. These results confirm MASHA's capability for high-resolution isotope identification in low-yield experiments.

1 Experimental Setup

The MASHA setup is built to facilitate the separation and identification of heavy and superheavy isotopes through a combination of mechanical, thermal, ionizing, and magnetic systems. At the core of the system is a rotating target wheel which holds up to six thin targets composed of isotopically enriched ^{148}Sm, ^{166}Er, or ^{242}Pu, each deposited on a titanium foil. The wheel is driven by a high-speed motor and rotates at a frequency of 25 Hz to evenly distribute heat across all target surfaces during beam exposure. When bombarded with an ion beam, nuclear reactions occur at the target interface, and the resultant reaction products are implanted into a graphite catcher located immediately behind the rotating target. The scheme is given in Figure 1. This catcher is resistively heated to approximately 2000 K and constructed from thermally expanded graphite to ensure both uniform heating and structural stability at high temperature [1][2]. The reaction products diffuse from the hot catcher into a transfer line that leads to the electron cyclotron resonance (ECR) ion source. To prevent atoms from adhering to internal surfaces and being lost before ionization, all relevant internal surfaces are coated with titanium nitride (TiN), a chemically inert and thermally resilient material. Once inside the ECR ion source, which operates at 2.45 GHz using microwave energy, the atoms are exposed to a stabilized plasma. Ionization predominantly yields singly charged ions, which are then extracted by a three-electrode electrostatic lens and accelerated to an energy of 38 keV which ensures that the ions are efficiently prepared for mass separation.

Mass separation is accomplished through a magneto-optical system made up of dipole magnets and electrostatic lenses. Depending on the experimental goals, the operator can choose between two modes: a high-efficiency mode with roughly 60% transmission and mass resolving power of $M/\Delta M \approx 1700$, or a high-resolution mode with reduced transmission (around 38%) but improved mass resolution of $M/\Delta M \approx 3000$. These modes allow for flexibility in detecting either rare isotopes or resolving closely spaced mass peaks.

At the final stage, the mass-separated ions are directed to a position-sensitive silicon-strip detector. This detector consists of a 192-strip frontal module supported by additional 64- and 16-strip side modules to enhance angular coverage. Operating at 40 V bias, the detector offers an energy resolution of around 25 keV, which is sufficient for precise alpha-spectroscopy. The system's geometry ensures high efficiency and spatial resolution, which are essential for reconstructing decay events, which supplies valuable superheavy element decay information [3][4].

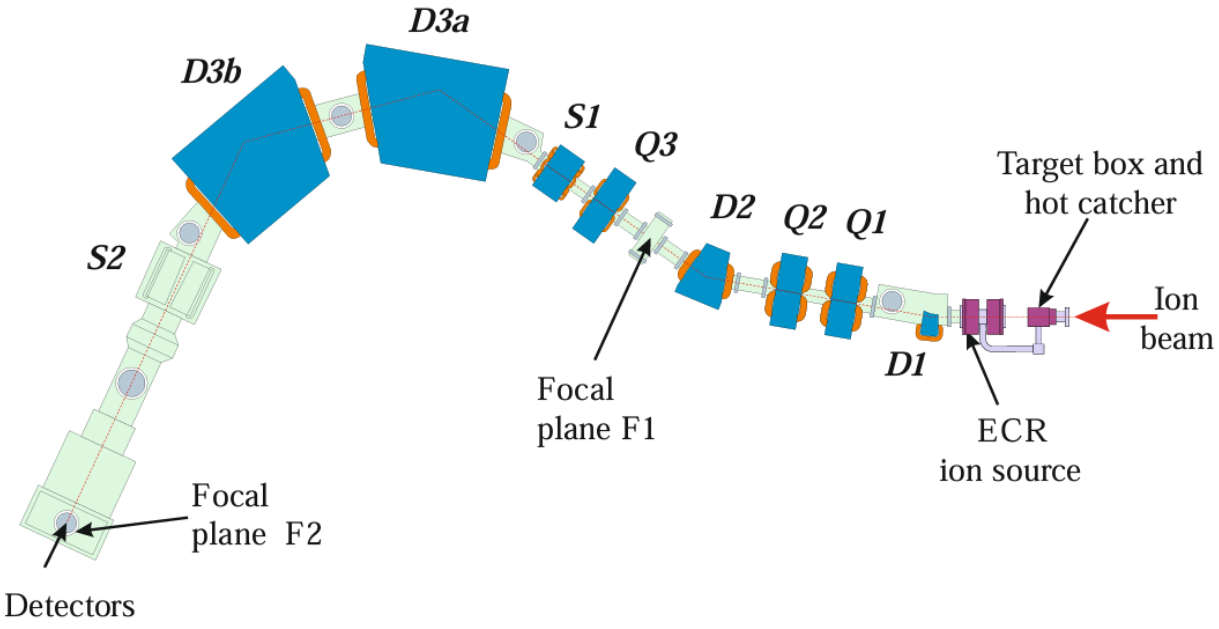

Figure 1: Scheme of the MASHA setup. D objects for dipole magnets, Q objects for quadrupole lenses and S objects for sextupole lenses.

2 Experimental Procedure

For each reaction system under study, the procedure began with the irradiation of the chosen target using either a ^{40}Ar or ^{48}Ca ion beam from the U-400M cyclotron. The beam energy was tuned depending on the reaction: typically between 5 and 7 MeV per nucleon for ^{40}Ar, and approximately 7.3 MeV per nucleon for ^{48}Ca. Beam alignment and current were continuously monitored using upstream diagnostic devices. If beam parameters deviated from acceptable limits, the control system would automatically shut down the beam to protect the experimental components [5].

During irradiation, nuclear reactions occurred at the target and the resulting products were implanted into the hot catcher. High temperature facilitated their release as neutral atoms, which were transported through the TiN-coated transfer system into the ECR ion source for ionization. The resulting ion beam, separated by mass-to-charge ratio, was directed toward the silicon-strip detector where decay events were recorded.

The data acquisition system continuously collected energy and position information from the detector strips. After the experiment, raw data were processed to remove baseline offsets and to extract peak energies. Alpha peaks were fitted using Gaussian functions to determine their centroids and full-width at half-maximum values.

Processed results were presented in the form of alpha-energy spectra and position–energy heatmaps. These visualizations allowed for precise identification of isotopes based on their decay energy and spatial localization within the detector array. The combination of thermal, ion-optical, and electronic systems in this setup allowed for efficient, time-resolved spectroscopy of short-lived neutron-rich isotopes.

3 Results

Measured alpha-decay energies for each reaction system are summarized in the following tables. Plots and heatmaps, which are referenced in the discussion below, will be inserted to support the identification of decay channels, spectral resolution, and background suppression.

3.1 ^{40}Ar+^{148}Sm

The spectrum obtained from this reaction showed a sequence of well-resolved alpha peaks that correspond to known mercury isotopes. Their decay signatures were clearly identified both in the 1D energy spectra and in the 2D position–energy plots. The table below shows the comparison between measured and theoretical values. In the heatmap, the peaks appear as localized high-intensity zones along distinct strip regions, confirming their origin. Spectroscopy results of produced isotopes and their daughters are given in Figure 2, a for ^{180}Hg, b for ^{181}Hg, c for ^{182}Hg, d for ^{183}Hg, e for ^{184}Hg, f for ^{185}Hg. Also, heatmap of produced isotopes are given in Figure 3.

Table 1: Alpha-decay energies for ^{40}Ar+^{148}Sm.

Isotope	$T_{1/2}$ (s)	Measured Energy (keV)	Theoretical Energy (keV)
Hg^{180}	2.58	6119	6119
Hg^{181}	10.83	6000	6006
Hg^{182}	9.40	5859	5867
Hg^{183}	30.9	5890	5904
Hg^{184}	49.1	5530	5535
Hg^{185}	82.8	5648	5653

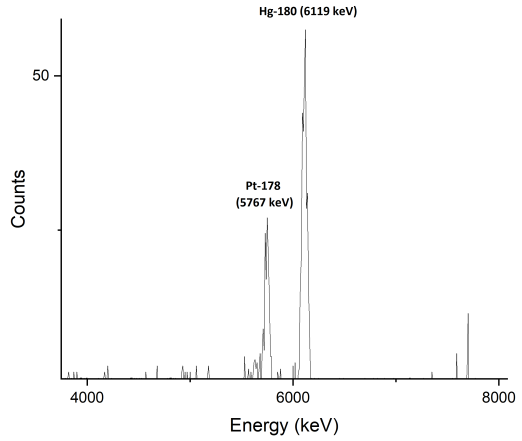

(a) ^{180}Hg

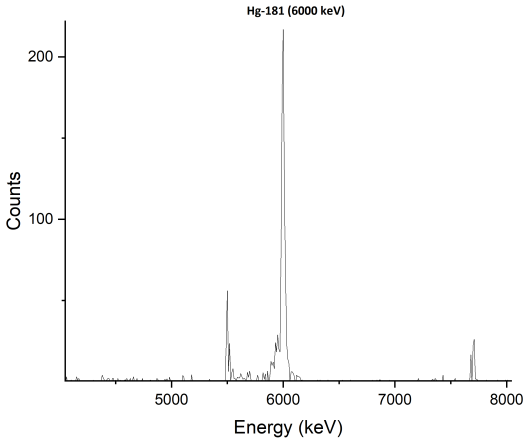

(b) ^{181}Hg

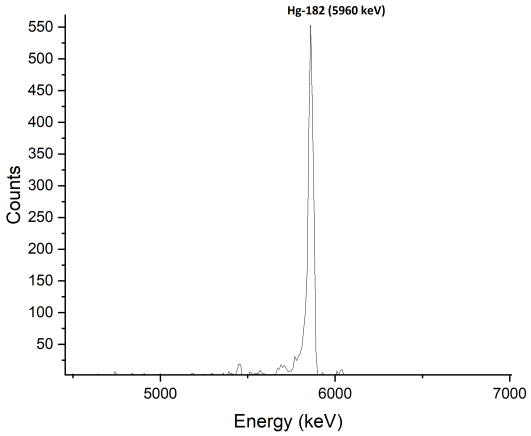

(c) ^{182}Hg

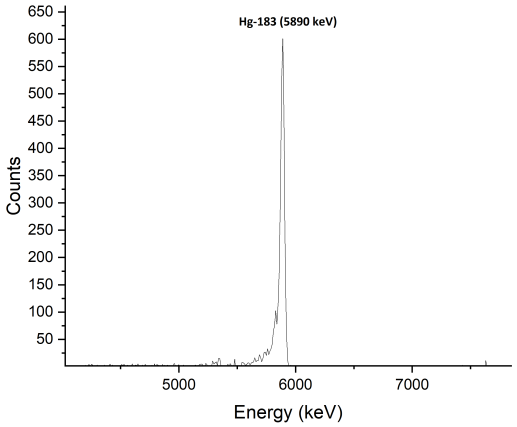

(d) ^{183}Hg

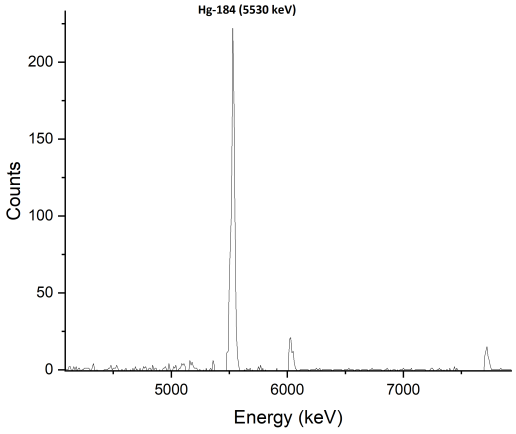

(e) ^{184}Hg

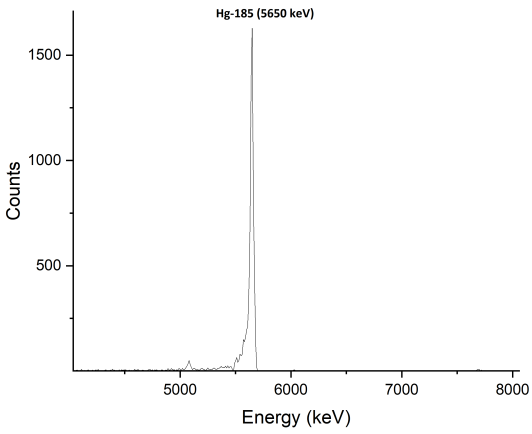

(f) ^{185}Hg

Figure 2: Alpha spectra and heatmaps for ^{180}Hg to ^{185}Hg. Subfigures (a) through (f) correspond to individual isotopes.

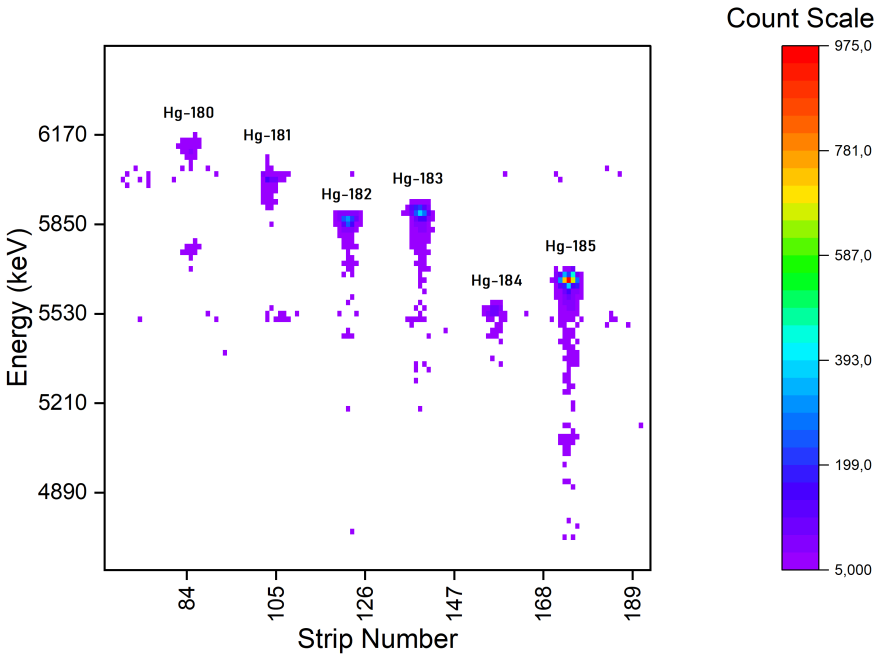

Figure 3: Heatmap of Hg isotopes.

3.2 ^{40}Ar+^{166}Er

This reaction populated several radon and polonium isotopes, visible as distinct structures in both the energy spectrum and position–energy heatmap. As seen in Table 2, experimental energies closely follow theoretical expectations. The decay chains appeared sequentially across neighboring strips, suggesting spatial consistency and allowing better background discrimination. The heatmap provides a visual confirmation of isotope assignment through strip localization.

Table 2: Alpha-decay energies for ^{40}Ar+^{166}Er.

Isotope	$T_{1/2}$ (s)	Measured Energy (keV)	Theoretical Energy (keV)
Rn^{201}	7.1	6722	6725
Rn^{202}	10	6629	6639
Rn^{203}	28	6499	6549
Rn^{204}	74.4	6399	6419
Rn^{205}	170	6269	6262
Po^{197}	25.8	6276	6383
Po^{198}	106.2	6182	6182
Po^{199}	250.2	5952	6059

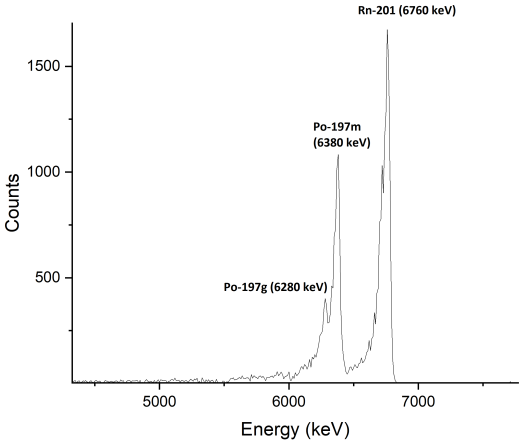

(a) ^{201}Rn

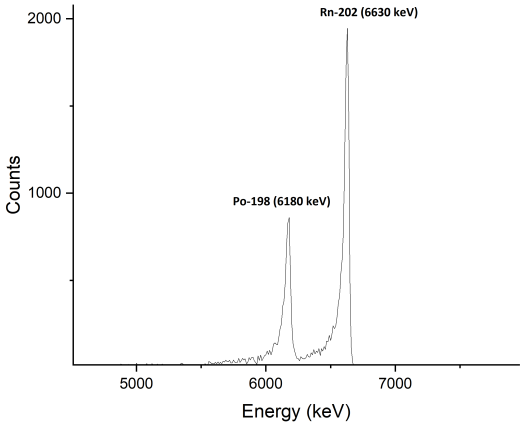

(b) ^{202}Rn

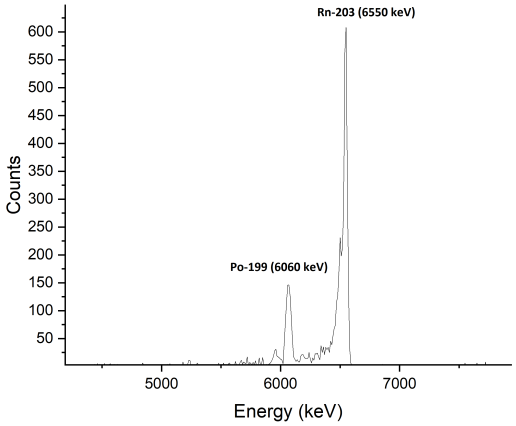

(c) ^{203}Rn

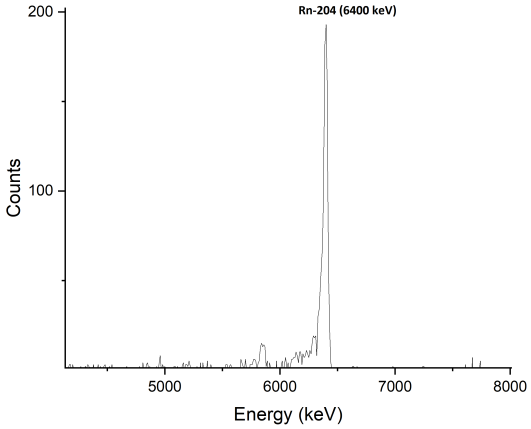

(d) ^{204}Rn

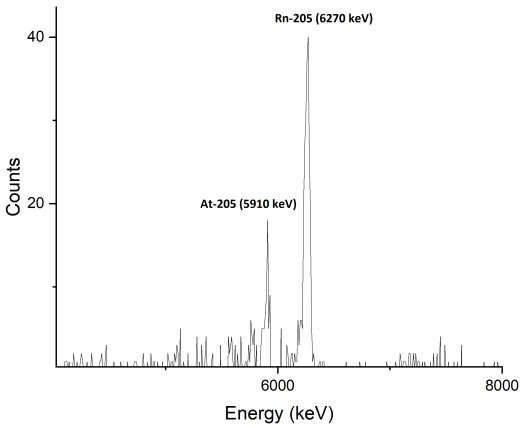

(e) ^{205}Rn

Figure 4: Alpha spectra and heatmaps for ^{201}Rn to ^{205}Rn. Subfigures (a) through (e) correspond to individual isotopes.

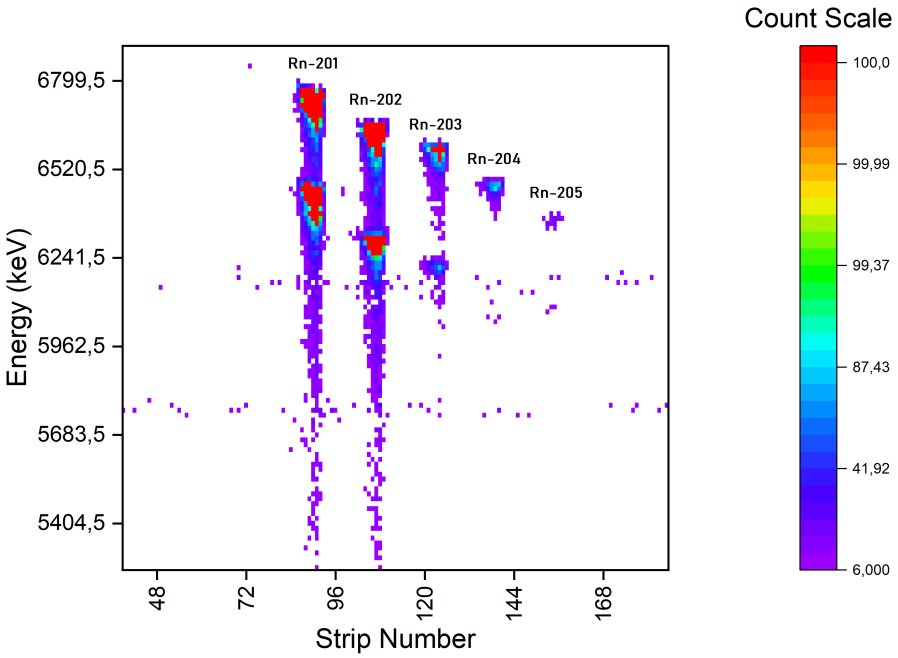

Figure 5: Heatmap of Rn isotopes.

3.3 ^{48}Ca+^{242}Pu

Prior to correction, this dataset showed an artificial compression in the energy spectrum due to a missing digit in energy calibration. After multiplying the energy values by ten, the expected peaks were clearly visible and aligned with theoretical values. The corrected spectrum reveals a consistent structure across strips. Table 3 outlines the matched decay energies, while the corresponding heatmap highlights areas of high count concentration corresponding to these peaks.

Table 3: Alpha-decay energies for ^{48}Ca+^{242}Pu.

Isotope	$T_{1/2}$	Measured Energy (keV)	Theoretical Energy (keV)
Rn^{212}	1434 s	6249	6264
Rn^{218}	0.00035 s	7110	7129
Rn^{219}	3.96 s	6789 / 6405	6819 / 6425
Rn^{222}	36.17 s	6591	6559
Po^{214}	0.000163 s	7658	7686
Po^{210}	138 d	5277	5304
Po^{215}	0.000178 s	7357	7386
Bi^{210}	5 d	4117	4100
Bi^{211}	128.4 s	6602 / 6250	6622 / 6250

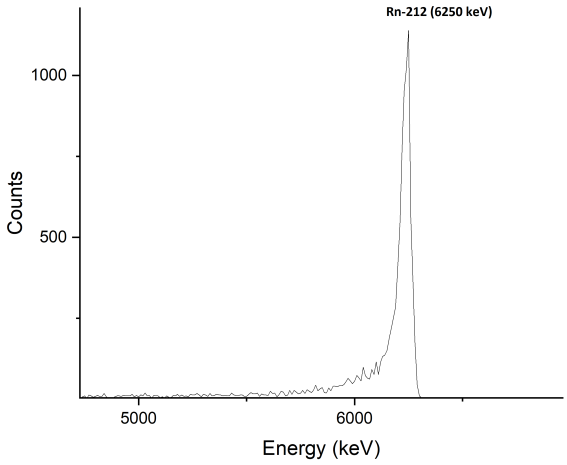

(a) ^{212}Rn

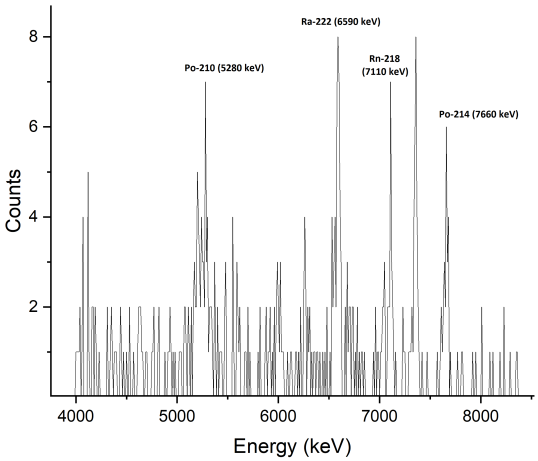

(b) ^{218}Rn

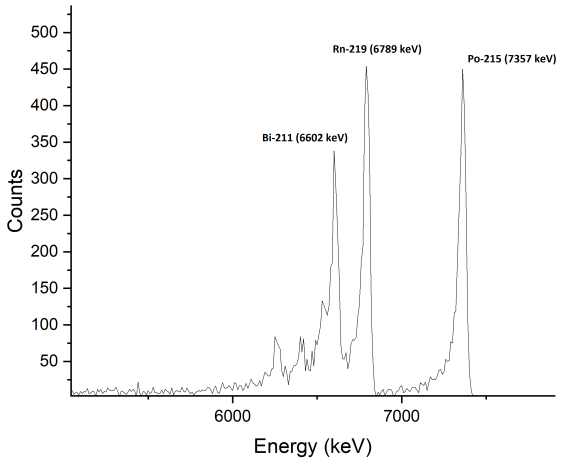

(c) ^{219}Rn

Figure 6: Alpha spectra and heatmaps for ^{212}Rn, ^{218}Rn and ^{219}Rn. Subfigures (a) through (c) correspond to individual isotopes.

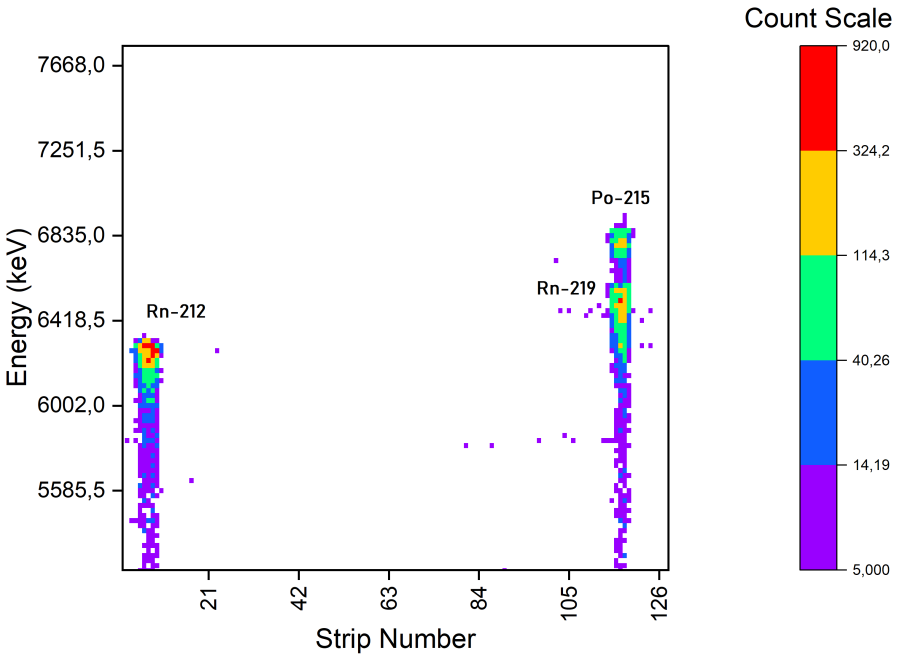

Figure 7: Heatmap of ^{212}Rn and ^{219}Rn isotopes.

4 Discussion and Conclusion

The experimental data obtained from the three investigated reaction systems confirm a strong correspondence between measured alpha-decay energies and their theoretical predictions. In all cases, the deviation remained within 0.5%, indicating reliable energy calibration and adequate resolution for distinguishing closely spaced isotopic lines.

In the ^{40}Ar+^{148}Sm fusion reaction, the identification of mercury isotopes through sharp and isolated alpha peaks provided clear benchmarks for calibration, as can be seen from Figure. The results from the ^{40}Ar+^{166}Er system further supported this trend, demonstrating successful detection of radon and polonium isotopes, which were distributed predictably across detector strips. These isotopes displayed consistent spatial groupings in the 2D heatmaps, which strengthened their assignments and reduced the possibility of background misinterpretation.

The ^{48}Ca+^{242}Pu multinucleon transfer experiment presented a technical challenge due to a misrecorded energy scale. Upon correction, the spectrum and spatial data clearly revealed expected radon and polonium decays. This emphasized the importance of accurate data validation, while also confirming the robustness of the recorded signals, which remained interpretable despite the scaling error.

Overall, the analysis of experimental data showed good alignment with theoretical expectations and demonstrated that the MASHA-based procedure is capable of resolving isotopes with short half-lives and low yields. The clarity of spectral lines, along with consistent spatial patterns, allowed confident isotope identification without ambiguity. This investigation successfully validated the experimental data quality for all three systems without needing to evaluate or speculate on the performance of individual hardware components.

References

[1] V. Yu. Vedeneev et al. "The current status of the MASHA setup". In: *Hyperfine Interactions* 238.1 (Jan. 2017). ISSN: 1572-9540. DOI: 10.1007/s10751-017-1395-9. URL: http://dx.doi.org/10.1007/s10751-017-1395-9.

[2] E. V. Chernysheva et al. "Determination of Separation Efficiency of the Mass-Spectrometer MASHA by Means of Measurement of Absolute Cross-Sections of Evaporation Residues". In: *Exotic Nuclei*. WORLD SCIENTIFIC, Nov. 2019, pp. 386–390. DOI: 10.1142/9789811209451_0054. URL: http://dx.doi.org/10.1142/9789811209451_0054.

[3] Heinz W Gäggeler. "Mendeleev's principle against Einstein's relativity: news from the chemistry of superheavy elements". In: *Russian Chemical Reviews* 78.12 (Dec. 2009), pp. 1139–1144. ISSN: 1468-4837. DOI: 10.1070/rc2009v078n12abeh004051. URL: http://dx.doi.org/10.1070/RC2009v078n12ABEH004051.

[4] Sergey N. Dmitriev et al. "Chemical identification of dubnium as a decay product of element 115 produced in the reaction 48Ca + 243Am". In: *Mendeleev Communications* 15.1 (Jan. 2005), pp. 1–4. ISSN: 0959-9436. DOI: 10.1070/mc2005v015n01abeh002077. URL: http://dx.doi.org/10.1070/MC2005v015n01ABEH002077.

[5] A. M. Rodin et al. "Features of the Solid-State ISOL Method for Fusion Evaporation Reactions Induced by Heavy Ions". In: *Exotic Nuclei*. WORLD SCIENTIFIC, Nov. 2019, pp. 437–443. DOI: 10.1142/9789811209451_0062. URL: http://dx.doi.org/10.1142/9789811209451_0062.